

A photometric-spectroscopic study of the infrared-excess eclipsing binary V2364 Cyg

Hui-Yu Yuan¹, Lin-Qiao Jiang², Hai-Feng Dai¹, Shuang Wang¹ and Yuan-Gui Yang^{1*}

¹ Information College & School of Physics and Electronic Information, Huaibei Normal University, Huaibei 235000, China; yygcn@163.com

² Artificial Intelligence Key Laboratory of Sichuan Province, Sichuan University of Science & Engineering, Zigong 643000, China

Received 2020 April 17; accepted 2020 July 2

Abstract The eclipsing binary V2364 Cyg is an A7V-type contact binary with a period of 0.5921 d. We present six spectra from *LAMOST* and *BVR_c* light curves (LCs), which are simultaneously analyzed to obtain the absolute physical parameters. The first light maxima are brighter than the second ones by up to 0^m038, 0^m036 and 0^m024 for *BVR_c* bands, respectively. These distorted LCs are modeled by a cool spot on the less massive component. Its mass ratio and over-contact degree are $q = 0.319(\pm 0.004)$ and $f = 28.4\%(\pm 1.0)\%$ respectively. From the mass-luminosity diagram, the primary component is a normal main-sequence star, while the secondary one is a subgiant star. From the (*O* – *C*) curve, the orbital period secularly decreases at a rate $dP/dt = -1.62(\pm 0.03) \times 10^{-7} \text{ d yr}^{-1}$, which is mainly attributed to mass loss via stellar wind from the binary system. This may result in the observed infrared excess in the *W4* band.

Key words: stars: circumstellar matter — stars: binaries: close — stars: individual (V2364 Cyg)— mass loss — infrared excess.

1 INTRODUCTION

Close binary (CB) stars may provide the most accurate parameters with uncertainties less than 3 percent, which have served as fundamental benchmarks for stars (Andersen 1991; Torres et al. 2010). They are widely distributed in open and globular clusters (Gimenez & Clausen 1996; Kaluzny & Krzeminski 1993; Milone et al. 1995), and the Large and Small Magellanic Clouds (LMC, Davidge 1987; SMC, Hoffmann et al. 1978), and are even used to measure accurate distances to nearby galaxies (Pietrzyński et al. 2013; Bonanos 2013). This kind of high frequency of occurrence offers a way to probe the stellar formation process. CBs were theoretically predicted to evolve from detached configuration into contact ones by three subtypes of case A binary evolution (Jiang 2020). Yildiz & Doğan (2013) proposed that binary systems with an initial mass higher than $1.8(\pm 0.1) M_{\odot}$ become A-subtype while systems with initial masses lower than this become W-subtype. Recently, statistical investigations of contact binaries have been performed by several authors, such

as Liu et al. (2018), Kouzuma (2019) and Zhang et al. (2020). However, some problems associated with CBs still remain open (see Zinnecker 2003; Tokovinin 2008; Boss 2014). Early-type eclipsing binaries (EBs) may be a unique laboratory to study some complicated physical processes, such as stellar wind (Hilditch 2001), X-ray emission (Brickhouse et al. 2005; Chen et al. 2006; He et al. 2019) and infrared excess (Scaltriti et al. 1993). Therefore, it is very important to determine absolute parameters for an early-type contact binary. V2364 Cyg is chosen as a target for investigation due to its possible magnetic activity on the less massive component, mass transfer, mass loss and infrared excess.

The object V2364 Cyg (= GSC 3551–1708) was identified as a variable star by the ROTSE project (Akerlof et al. 2000)¹, whose light curve (LC) implies that this star is a W UMA-type binary. Nelson et al. (2002) performed the subsequent observation and determined an orbital period of 0.5921376 d. Based on the color index of $B - V = 0^m38$, they estimated its spectral type to

* Corresponding author

¹ The Robotic Optical Transient Search Experiment (ROTSE), see <http://www.umich.edu/~rotse/>

Table 1 RVs and Effective Temperatures for the Primary Component

HJD	Phase	RV (km s ⁻¹)	Error (km s ⁻¹)	Temperature (K)
2456798.2896	0.7275	+8.54	14.73	7406 ± 43
2456918.0368	0.9567	+3.59	6.59	7314 ± 8
2457297.9861	0.6155	+3.10	8.58	7275 ± 11
2457298.0201	0.6729	+11.10	10.99	7284 ± 15
2457919.2458	0.7275	+27.60	12.14	7302 ± 21
2457919.2715	0.8431	+19.59	10.33	7279 ± 17

be *F4V* with a temperature of 6820 K. From the *RI* LCs, they deduced the photometric solution with a cool spot on the less massive component. The results imply that V2364 Cyg is an A-subtype contact binary with a mass ratio of $q = 0.306(\pm 0.002)$. From *Gaia* Data Release 2 (Gaia Collaboration et al. 2018), the stellar parallax is $1.4774(\pm 0.0282)$ mas, corresponding to a distance of $d = 676.9(\pm 12.9)$ pc from Earth. Although several times of minimum light have been reported in some literature, the period analysis has been neglected up to now.

New photometric and spectroscopic observations were gathered concerning the contact binary V2364 Cyg in this study. Multicolor LCs and a radial velocity (RV) curve are presented in Section 2. Absolute parameters were determined from new RV and LCs by employing the Wilson-Devinney program² in Section 3. From all available times of minimum light, we construct the $O - C$ (e.g., observed minus calculated times of minimum light) curve in Section 4 to study its orbital period variations. In the final section, we discuss the evolutionary state and spectral energy distribution (SED), and mass loss from this binary system.

2 OBSERVATIONS

2.1 LAMOST Spectra for V2364 Cyg

From the *LAMOST DR6* v1 database³, we searched six low-resolution spectra for V2364 Cyg from 2014 to 2019, which are displayed in Figure 1(a). Based on the online spectra, we obtained RVs, uncertainties and temperatures, which are tabulated in Table 1. Heliocentric Julian Dates (HJDs) are taken from the times observations were conducted. The RV curve is plotted in Figure 1(b), which indicates that it is associated with the primary component because the RVs for the secondary component could not be obtained from the low-precision spectra. The mean effective temperature is $T_p = 7310(\pm 19)$ K for the primary component. Its spectral type is determined

to be *A7V*, rather than *F4* deduced from the color index (Nelson et al. 2002). Therefore, V2364 Cyg is an early-type contact binary.

2.2 CCD Photometry

BVR_c photometry for V2364 Cyg was performed on 2018 September 4, 5 and 6 by using the 85-cm telescope at Xinglong Station (XLS) of National Astronomical Observatories, Chinese Academy of Sciences (NAOC). The CCD camera was mounted at the primary focus of this telescope (Zhou et al. 2009). The standard *UBVR_cI_c* filters were applied. Reductions for all effective images were performed by the IRAF software packages in standard mode, including zero, flat-fielding and extinction corrections. Then magnitudes were determined by the aperture photometry.

During the observing process, GSC 3551–1771 and GSC 3551–2312 were chosen as the comparison and check stars respectively. Exposure times are 50 s, 40 s and 30 s for *BVR_c* bands, respectively. The individual observations, i.e., HJD versus Δm , are listed in Table 2. The standard deviations for all data are better than 0^m007 , 0^m004 and 0^m003 for *BVR_c* filters respectively. The complete LCs are displayed in Figure 2(a), in which phases are computed by an orbital period of 0.5921376 d (Nelson et al. 2002). Its variable amplitude is approximated by $\sim 0^m57$. Other properties of LCs are listed in Table 3. From Figure 2(a), Max.I (i.e., ph=0.25) is brighter than Max.II (i.e., ph=0.75) by approximately up to $\simeq 0^m03$. The unequal heights between both maxima in LCs may be the O’Connell effect (Milone 1968; Davidge & Milone 1984). Figure 3 displays the intrinsic light variability in the *V* band, in which we used the data observed by Nelson et al. (2002)⁴. The small-amplitude light variability evidently occurs around Max.II (i.e., phase 0.75). The comparison results are given in Table 3, including variable amplitude, Min.I–Min.II and Max.I–Max.II. The noticeable variation with time may result from cool-spot activity on the convective envelope. This situation occurs in other contact binaries, such as GU Mon (Yang et al. 2019), GN Boo (Wang et al. 2015), OO Aql (Li et al. 2016), V410 Aur (Luo et al. 2017) and DZ Psc (Yang et al. 2013).

3 PHOTOMETRIC-SPECTROSCOPIC ELEMENTS

BVR_c LCs and the primary’s RVs were simultaneously analyzed by the 2015 version of the Wilson-Devinney pro-

² <ftp://ftp.astro.ufl.edu/pub/wilson/lcdc2015>

³ <http://dr6.lamost.org>

⁴ Nelson et al. (2002) published 257 data in *V* band, observed on five nights in October 2001, which can be seen at the website <https://konkoly.hu/pub/ibvs/5201/5285-t4.txt>.

Table 2 *BVR* Photometric Observations for V2364 Cyg in 2018

<i>B</i> band		<i>V</i> band		<i>R</i> band	
HJD	Δm	HJD	Δm	HJD	Δm
2458366.0549	-0.262	2458366.0554	-0.003	2458366.0559	+0.176
2458366.0565	-0.251	2458366.0571	+0.009	2458366.0576	+0.183
2458366.0582	-0.246	2458366.0588	+0.013	2458366.0593	+0.184
2458366.0599	-0.239	2458366.0605	+0.023	2458366.0610	+0.192
2458366.0616	-0.236	2458366.0622	+0.020	2458366.0627	+0.197
2458366.0633	-0.230	2458366.0639	+0.032	2458366.0644	+0.200
2458366.0650	-0.218	2458366.0656	+0.037	2458366.0661	+0.210
2458366.0667	-0.208	2458366.0673	+0.046	2458366.0677	+0.224
2458366.0683	-0.202	2458366.0689	+0.049	2458366.0694	+0.231
2458366.0711	-0.188	2458366.0717	+0.075	2458366.0721	+0.236
2458366.0727	-0.182	2458366.0732	+0.079	2458366.0737	+0.256
2458366.0743	-0.174	2458366.0748	+0.083	2458366.0753	+0.259

This table is available in its entirety in machine-readable form at <http://www.raa-journal.org/docs/Supp/ms4698table2.txt>. A portion is shown here for guidance regarding its form and content.

Table 3 Properties of LCs for V2364 Cyg

Parameters	<i>LC</i> in 2018	<i>LC</i> in 2001 ^a
Number of data	366(<i>B</i>), 361(<i>V</i>), 362(<i>R_c</i>)	272(<i>V</i>)
Reference epoch (t_0)	HJD 2458368.1985	HJD 2452186.9014
Var. amplitude ^b (mag)	0.582(<i>B</i>), 0.569(<i>V</i>), 0.580(<i>R_c</i>)	0.532(<i>V</i>)
Min. I-Min. II (mag)	+0.120(<i>B</i>), +0.100(<i>V</i>), +0.082(<i>R_c</i>)	+0.055(<i>V</i>)
Max. I-Max. II (mag)	-0.038(<i>B</i>), -0.036(<i>V</i>), -0.024(<i>R_c</i>)	-0.025(<i>V</i>)

^a The *V*-band observations are referenced from IBVS 5285 (Nelson et al. 2002). ^b The variable amplitude is the magnitude difference between Min. I and Max. I, in which Min. I, Max. I, Min. II and Max. II refer to the values at phases of 0.00, 0.25, 0.50 and 0.75, respectively.

Table 4 Spectroscopic-photometric Elements for V2364 Cyg

Parameters	Sol. 1	Sol. 2	Sol. 3
	(without a spot)	(with a hot spot)	(with a cool spot)
Mass ratio, $q = M_2/M_1$	0.305 ± 0.005	0.315 ± 0.005	0.319 ± 0.004
Orbital inclination, i ($^\circ$)	80.92 ± 0.18	80.30 ± 0.16	81.60 ± 0.11
Separation, a (R_\odot)	3.95 ± 0.15	3.96 ± 0.15	3.96 ± 0.15
Velocity of center of mass, V_0 (km s^{-1})	49.85 ± 8.86	50.22 ± 7.44	52.96 ± 9.07
The primary's temperature, T_1 (K)		7310 ± 19	
Modified dimensionless surface potential, $\Omega_{1,2}$	2.4190 ± 0.0044	2.4230 ± 0.0018	2.4515 ± 0.0019
The secondary's temperature, T_2 (K)	6527 ± 20	6511 ± 8	6542 ± 5
Bolometric limb darkening coefficient, X_{2bol}, Y_{2bol}	0.645, 0.241	0.645, 0.240	0.645, 0.241
Bandpass limb darkening coefficient, x_{2B}, y_{2B}	0.803, 0.254	0.803, 0.252	0.802, 0.255
Bandpass limb darkening coefficient, x_{2V}, y_{2V}	0.710, 0.285	0.711, 0.284	0.709, 0.285
Bandpass limb darkening coefficient, x_{2R_c}, y_{2R_c}	0.638, 0.287	0.639, 0.287	0.637, 0.288
^a Bandpass luminosity ratio, ℓ_{1B}	0.8423 ± 0.0064	0.8387 ± 0.0041	0.8352 ± 0.0026
Bandpass luminosity ratio, ℓ_{1V}	0.8214 ± 0.0064	0.8170 ± 0.0039	0.8142 ± 0.0028
Bandpass luminosity ratio, ℓ_{1R_c}	0.8081 ± 0.0064	0.8031 ± 0.0041	0.8007 ± 0.0033
Pole relative radius, r_{1pole}	0.4665 ± 0.0023	0.4681 ± 0.0014	0.4635 ± 0.0023
Side relative radius, r_{1side}	0.5046 ± 0.0024	0.5070 ± 0.0018	0.5011 ± 0.0025
Back relative radius, r_{1back}	0.5339 ± 0.0027	0.5380 ± 0.0020	0.5317 ± 0.0027
^b Point relative radius, r_{1point}	0.6193 ± 0.0016	0.6162 ± 0.0015	0.6150 ± 0.0012
Pole relative radius, r_{2pole}	0.2740 ± 0.0014	0.2792 ± 0.0012	0.2812 ± 0.0014
Side relative radius, r_{2side}	0.2871 ± 0.0015	0.2929 ± 0.0013	0.2950 ± 0.0015
Back relative radius, r_{2back}	0.3304 ± 0.0017	0.3394 ± 0.0019	0.3405 ± 0.0017
Point relative radius, r_{2point}	0.3807 ± 0.0010	0.3848 ± 0.0009	0.3850 ± 0.0008
Longitude, θ (radian)	–	6.16 ± 0.04	4.82 ± 0.02
Angular radius, γ (radian)	–	0.24 ± 0.03	0.615 ± 0.096
Dimensionless temperature factor, T_{spot}/T_{pri}	–	1.35 ± 0.04	0.875 ± 0.039
The sum of squared residual, $\Sigma(o - c)_i^2$	1.443×10^{-3}	1.359×10^{-3}	0.901×10^{-3}

^aBandpass luminosity ratio is $\ell_{1i} = L_{1i}/(L_{1i} + L_{2i})$, in which i refers to *B*, *V* or *R_c* band. ^bThe point relative radii r_{point} ends at the inner Lagrange point L_1 , i.e., $r_{point} = x_1$ for a given mass ratio (see p.134 of Kopal 1959).

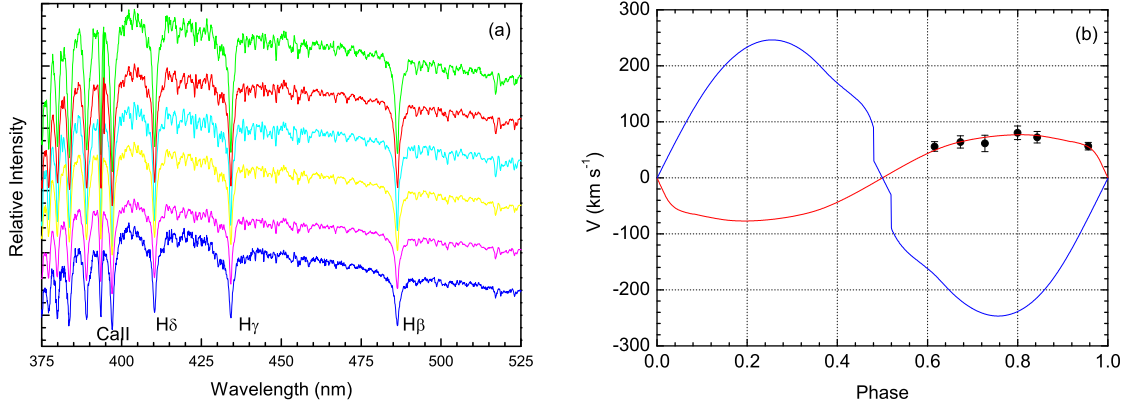


Fig. 1 The low-precision spectra (a) and RVs (b) for V2364 Cyg, which were observed by *LAMOST*. In Fig. 1(b), the continuous *red* and *blue* lines are theoretical RV curves, which are computed by Sol.3 of Table 4. All observed and calculated values for RVs are subtracted by the velocity of the center of mass, $V_0 = 52.96 \text{ km s}^{-1}$.

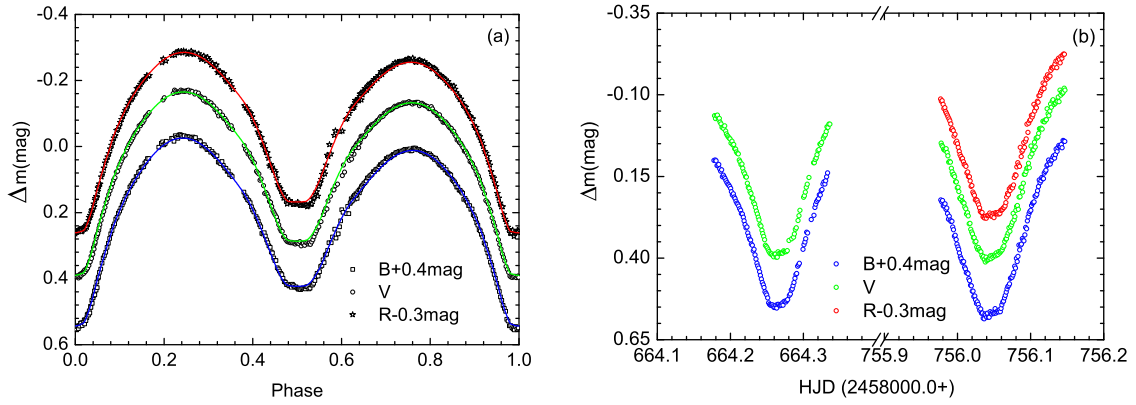


Fig. 2 (a) *BVR* LCs were observed on 2018 Sep.; (b) two primary eclipses were identified on 2019 June 29 and September 29. The *solid* lines in (a) are computed by Sol.3 in Table 4.

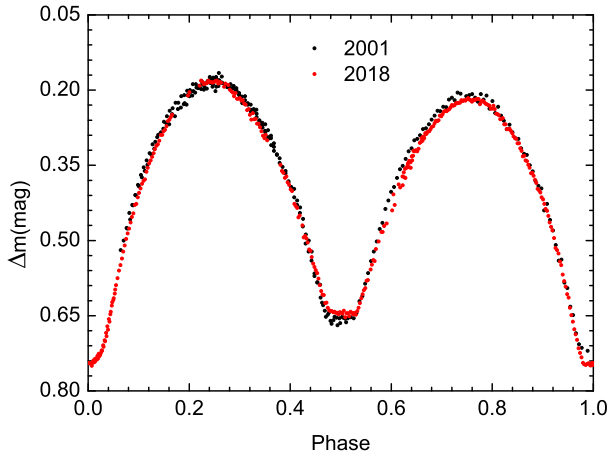


Fig. 3 The intrinsic light variability in the *V*-band LCs, whose data in 2001 are taken from Nelson et al. (2002).

gram (Wilson & Devinney 1971; Wilson & van Hamme 2014). We first fixed the bolometric albedos (Von Zeipel 1924; Ruciński 1969) and gravity darkening coefficients (Lucy 1967), which are appropriate for a star with

convective or radiative envelope. Based on the stellar effective temperature, the logarithmic monochromatic and bolometric limb-darkening coefficients are interpolated into the tables from Van Hamme (1993). As usual, we choose seven adjustable parameters (i.e., separation a , systemic velocity V_0 , mass ratio q , orbital inclination i , dimensionless surface potential $\Omega_{1,2}$, mean surface temperature T_2 and bandpass luminosity L_1), in which the suffixes 1 and 2 refer to stars 1 and 2 respectively (Wilson & van Hamme 2016). Meanwhile, L_2 is computed by the stellar atmosphere model (Kurucz 1993).

Similarly to the Nelson et al. (2002) photometric solution, we adopted the contact configuration (i.e., mode 3) to analyze three-color LCs and RVs for V2364 Cyg. The mass ratio of $q = 0.306$ (Nelson et al. 2002) was chosen as an initial input parameter. The mean effective temperature of $T_1 = 7310(\pm 19) \text{ K}$ is averaged from the temperatures in Table 1. With the differential corrections program, we first derived a photometric-spectroscopic solution (i.e., Sol.1 without a spot), which is listed in

Table 5 Newly Determined Light Minimum Times

HJD	Error	Type	Filter
2458366.12899	± 0.00019	Pri.	B
2458366.12879	± 0.00020	Pri.	V
2458366.12845	± 0.00033	Pri.	R
2458368.19854	± 0.00018	Pri.	B
2458368.19844	± 0.00017	Pri.	V
2458368.19865	± 0.00020	Pri.	R
2458664.26520	± 0.00014	Sec.	B
2458664.26533	± 0.00017	Sec.	V
2458756.04416	± 0.00017	Pri.	B
2458756.04485	± 0.00017	Pri.	V
2458756.04447	± 0.00021	Pri.	R

Table 4. For V2364 Cyg, the orbital period decrease may be attributed to mass transfer from the primary to the secondary (see Sect. 5.3), which may cause a hot spot on the less massive component. On the other hand, Max. I of LCs in 2018 is brighter than Max. II up to $0^m 038$, $0^m 036$ and $0^m 024$ for BVR_c bands, respectively. Considering that the primary component is A7V-type, the asymmetry in LCs may be modeled by a cool spot on the late-type secondary component, which coincides with a single spot on star 2 from Nelson et al. (2002). Assuming a hot or cool spot is located on the equator of star 2 (i.e., latitude $\phi = 90^\circ$), three other parameters (i.e., longitude θ , angular radius γ and dimensionless temperature factor T_{spot}) of a spot are adjustable. Finally, we derived another two photometric-spectroscopic solutions, i.e., Sol.2 with a hot spot and Sol.3 with a cool spot, which are tabulated in Table 4. Due to a smaller sum of the squared residuals, we accepted Sol.3 as the final solution. The spot covers 9.2% of the area of the lower massive component. This kind of cool spot on the less massive component occurs on three other early-type contact binaries, such as DU Boo (Djurasević et al. 2013), V1073 Cyg (Ekmekçi et al. 2012) and V376 And (Djurasević et al. 2008). The final mass-ratio of $q = 0.319(\pm 0.004)$ is a little larger than the value of $q = 0.306(\pm 0.002)$ derived from Nelson et al. (2002). The fill-out factor for this binary is $f = 28.4(\pm 1.0)\%$. The theoretical RV curves are plotted as continuous lines in Figure 1(b), while the computed LCs are displayed as color lines in Figure 2(a).

4 ECLIPSE TIMINGS AND PERIOD ANALYSIS

As displayed in Figure 2(b), two primary eclipses were monitored with the 85-cm and 80-cm telescopes at XLS of NAOC (Zhou et al. 2009; Huang et al. 2012). From those new observations, several times of minimum light were determined by the method of Kwee & van Woerden (1956). The single-band eclipse timings along with their uncertainties are expressed in Table 5.

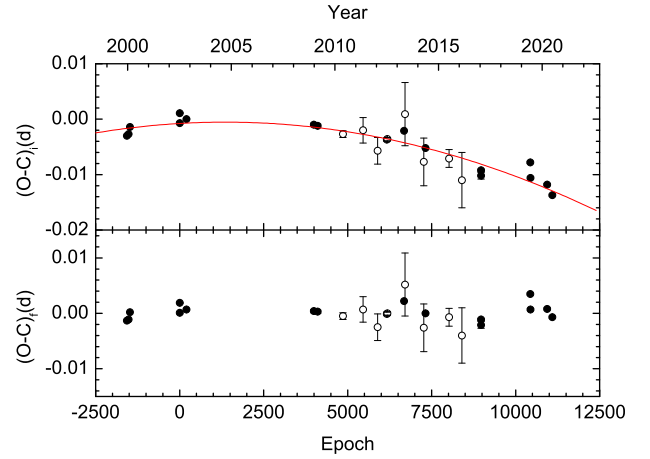


Fig. 4 The $O-C$ curve for V2364 Cyg. Open and solid circles refer to photometric and CCD measurements, respectively. The continuous line is plotted by Eq. (2).

From the $O-C$ gateway⁵, we compiled a total of 25 light minimum times, including 9 photoelectric and 16 CCD data. Table 4 lists those minimum times together with the measured errors. For four light minimum times, no uncertainties have been presented in literature (Nelson et al. 2002; Nagai 2013). Then we averaged the uncertainties of other CCD data as their uncertainties (i.e., 0.0013 d). During the fitting process, the weights for data were always inversely proportional to their measured uncertainties. With the Nelson et al. (2002) ephemeris as follows,

$$\begin{aligned} \text{Min. I} = & \text{HJD } 2452186.90143(10) \\ & + 0.5921376(5) \times E, \end{aligned} \quad (1)$$

we compute the initial residuals, $(O - C)_i$, which are listed in the sixth column of Table 4 and are depicted in the upper panel of Figure 4. From this figure, the $(O - C)_i$ curve evidently displays a secular period decrease, so we describe it with a downward parabola. By the linear least-squares method, we yield the quadratic ephemeris,

$$\begin{aligned} \text{Min. I} = & \text{HJD } 2452186.9006(2) + 0.59213636(2) \times E \\ & - 1.31(2) \times 10^{-10} \times E^2, \end{aligned} \quad (2)$$

in which the standard derivation in parentheses is in the unit of the last decimal place for the preceding quantity. The final residuals of $(O - C)_f$ are listed in Table 4, and are shown in the lower panel of Figure 4. From the quadratic coefficient of Equation (2), we can estimate a period decrease rate of $dP/dt = -1.62(\pm 0.03) \times 10^{-7} \text{ d yr}^{-1}$.

⁵ <http://var2.astro.cz/ocgate/>

Table 6 All Available Light Minimum Times for V2364 Cyg

HJD	Error	Epoch	Method	Min	$(O - C)_i$ (d)	$(O - C)_f$ (d)	References
2451257.8370	–	–1569.0	CCD	I	–0.0030	–0.0013	Nelson et al. (2002)
2451286.8520	–	–1520.0	CCD	I	–0.0027	–0.0011	Nelson et al. (2002)
2451311.7230	–	–1478.0	CCD	I	–0.0014	+0.0002	Nelson et al. (2002)
2452186.9007	± 0.0002	+0.0	CCD	I	–0.0007	+0.0001	Nelson et al. (2002)
2452189.5671	± 0.0001	4.5	CCD	II	+0.0011	+0.0019	Nelson et al. (2002)
2452307.9932	± 0.0001	204.5	CCD	II	+0.0000	+0.0007	Nelson et al. (2002)
2454551.0034	± 0.0003	3992.5	CCD	II	–0.0010	+0.0004	Nelson (2008)
2454617.9145	± 0.0003	4105.5	CCD	II	–0.0012	+0.0003	Nelson (2008)
2455066.4561	± 0.0006	4863.0	pe	I	–0.0027	–0.0005	Hübsher et al. (2010)
2455418.4816	± 0.0023	5457.5	pe	II	–0.0020	+0.0007	Hübsher (2011)
2455674.5767	± 0.0024	5890.0	pe	I	–0.0057	–0.0025	Huang et al. (2012)
2455838.3043	± 0.0003	6166.5	pe	II	–0.0037	–0.0001	Hübsher & Lehmann (2012)
2455848.3708	± 0.0003	6183.5	pe	II	–0.0036	+0.0000	Hübsher et al. (2012)
2456142.0717	–	6679.5	CCD	II	–0.0021	+0.0022	Nagai (2013)
2456157.4702	± 0.0057	6705.5	pe	II	+0.0009	+0.0052	Hübsher & Lehmann (2013)
2456490.5381	± 0.0043	7268.0	pe	I	–0.0077	–0.0026	Hübsher (2013))
2456520.4435	± 0.0001	7318.5	CCD	II	–0.0052	+0.0000	Hoňková et al. (2014)
2456933.4565	± 0.0016	8016.0	pe	I	–0.0071	–0.0007	Hübsher (2015)
2457161.4249	± 0.0050	8401.0	pe	I	–0.0110	–0.0040	Hübsher (2016)
2457498.9433	± 0.0006	8971.0	CCD	I	–0.0102	–0.0021	Nelson (2017)
2457499.5364	± 0.0002	8972.0	CCD	I	–0.0092	–0.0011	Juryšek et al. (2017)
2458366.1288	± 0.0002	10435.5	CCD	II	–0.0078	+0.0035	Present work
2458368.1985	± 0.0002	10439.0	CCD	I	–0.0106	+0.0007	Present work
2458664.2653	± 0.0002	10939.0	CCD	I	–0.0118	+0.0008	Present work
2458756.0445	± 0.0002	11094.0	CCD	I	–0.0137	–0.0007	Present work

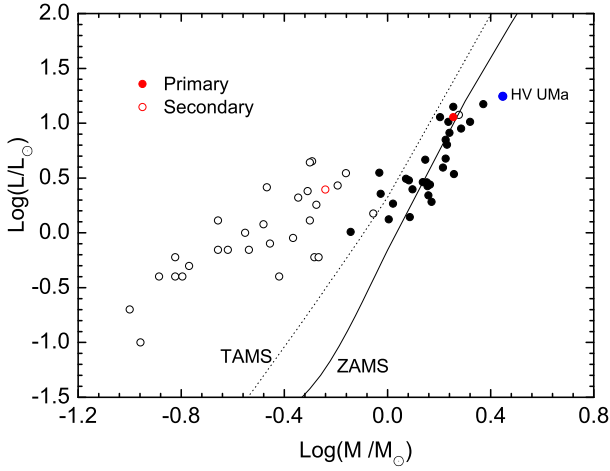


Fig. 5 The mass-luminosity diagram for V2364 Cyg, whose primary and secondary components are plotted as red solid and open circles respectively. The continuous and dotted lines are ZAMS and TAMS lines respectively with $z = 0.02$. The black symbols represent 29 A-type LTCBs referenced from Yakut & Eggleton (2005). The blue filled circle signifies the more massive component of HV UMa.

5 DISCUSSIONS

5.1 Absolute Parameters and Evolutionary State

From the solution with a cool spot in Table 4, we directly determined the absolute parameters for V2364 Cyg. The equivalent radius for each component R is computed from the relation of $(R/a)^2 = [2r_{pole}r_{side} + (r_{pole} +$

$r_{point})(r_{back} + r_{point})]/6$ (see p.134 of Kopal 1959). Then we obtained the radius of $R_1 = 2.11 \pm 0.08 R_\odot$ and $R_2 = 1.23 \pm 0.19 R_\odot$. By applying Kepler’s third law, $M_1 + M_2 = 0.0134a^3/P^2$, the masses are estimated to be $M_1 = 1.80 \pm 0.21 M_\odot$ and $M_2 = 0.57 \pm 0.07 M_\odot$. With the help of the Stefan-Boltzmann law, $L = 4\pi\sigma R^2T^4$, we derived the luminosities of $L_1 = 11.35 \pm 0.89 L_\odot$ and $L_2 = 2.48 \pm 0.19 L_\odot$. From those parameters, the secondary component of V2364 Cyg is more likely a subgiant star.

In order to determine the evolutionary state for V2364 Cyg, we constructed the zero age main sequence (ZAMS) and terminal age main sequence (TAMS) lines with $z = 0.02$ by the binary-star evolution code (Hurley et al. 2002). Two components are displayed in the mass-luminosity diagram in Figure 5, where 29 A-type low-temperature contact binaries (LTCBs; Yakut & Eggleton 2005) are marked as black filled and open circles. This kind of LTCB shares a common convective envelope. HV UMa is a contact binary with early-type components. Csák et al. (2000) argued that their adopted temperature of the primary component (i.e., 7000 K) is too cool and too faint for its mass (i.e., $2.8 M_\odot$). Thus its primary’s luminosity is too low so that it deviates from the ZAMS line (see Fig. 5 as a blue filled circle). For A-type W UMa binaries, the secondary’s overluminosity may result from its evolution from the initially more massive star (Yildiz & Doğan 2013;

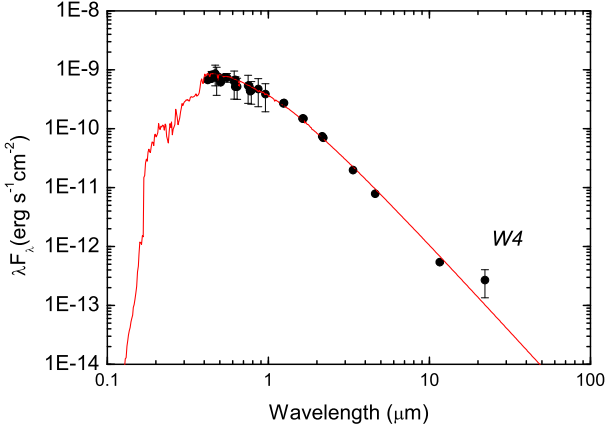


Fig. 6 The SED of V2364 Cyg. The *red line* is the combined atmospheric spectrum from two components. The *black solid circles* are measured fluxes for photometric bands, including the *W4* band (*Color version is online*).

Zhang et al. 2020). After a low-mass star (i.e., $M \leq 2.0 M_{\odot}$) has left the main sequence (MS), it becomes a subgiant, and a hydrogen-burning shell ignites just outside its helium core (Denissenkov & VandenBerg 2003). After ejecting its envelope in an advanced evolutionary stage (Stepień 2006), it may be a small helium star. The primary component of V2364 Cyg is located on the ZAMS line, which implies that it may be a normal MS star. Meanwhile, its secondary component largely lies above the TAMS line, indicating that its overluminosity is similar to that of an A-type contact binary. It may still be a subgiant star from its mass, radius and luminosity.

5.2 Spectral Energy Distribution

For the early-type star V2364 Cyg, mass loss from the binary system is inevitably through stellar wind (Castor et al. 1975; Abbott 1982). The circumstellar matter around the binary may result in the observed infrared excess. The broadband photometric data are taken from the *Vizier* query service⁶. Those measured fluxes and their associated derivations are listed in Table 7. We gave an uncertainty of 0.01 mag for the *W4* band, which is similar to the procedure by Stassun & Torres (2016). The observed SED is plotted in Figure 6, in which the infrared excess evidently occurs around the *W4* band.

In order to fit the observed SED, we adopted the standard stellar atmosphere model (Kurucz 1993). The total thermal radiation is attributed to two components. The flux density from the binary’s emissivity received at the Earth is,

$$\varepsilon = \left(\frac{R_1}{2d}\right)^2 \times F_{\nu,1} + \left(\frac{R_2}{2d}\right)^2 \times F_{\nu,2}, \quad (3)$$

⁶ <http://vizier.u-strasbg.fr/vizier/sed/>

in which R_1 and R_2 , and $F_{\nu,1}$ and $F_{\nu,2}$ are radii and radiative fluxes of stars 1 and 2, respectively. The theoretical SED is plotted in Figure 6 as a continuous line. For the *W4* band, the observed flux density of 1.98 mJy is larger than the computed flux density of 0.76 mJy. So, the infrared excess flux density approximates to 1.22 mJy, which could not result from the observed uncertainty, i.e., 50% for the measured fluxes assumed as the uncertainty even in a worse case. Infrared excess also exists in our previously studied binaries, i.e., CT Tau, GU Mon and V701 Sco (Yang et al. 2019), indicating that the circumbinary envelope may be generally constructed via mass loss due to stellar wind in this kind of early-type infrared-excess binary.

5.3 Secular Period Decrease for V2364 Cyg

From the previous period analysis, the period of V2364 Cyg is decreasing at a rate of $dP/dt = -1.62(\pm 0.03) \times 10^{-7} \text{d yr}^{-1}$. This situation also occurs in other early-type contact binaries, which are compiled in Table 8. From this table, its period decrease rate is a bit smaller than the values for three other binaries except for SV Cen⁷. For a contact binary, two components fill their Roche lobes. Mass is inevitably lost by stellar wind (Castor et al. 1975; Abbott 1982). Meanwhile, the binary system loses angular momentum due to escaping matter and magnetic braking for a late-type star with a convective envelope (Nanouris et al. 2011; Mestel & Spruit 1987). For V2364 Cyg, the secular period decrease may be attributed to the net effect of transferring mass between two components, losing mass and angular momentum from the binary system.

For the non-conservative evolution of this binary, we adopted the following equation (Erdem & Öztürk 2014),

$$\frac{\dot{P}}{P} = -2\frac{\dot{M}}{M} + 3\frac{M_1 - M_2}{M_1 M_2} \dot{M}_1 + 2\left(\frac{R_A}{a}\right)^2 \frac{M}{M_1 M_2} \dot{M}, \quad (4)$$

in which a and M are the separation between the two components and the total mass of the binary star respectively. For V2364 Cyg, the third term in Equation (4) may result from magnetic braking of the less massive component, which will become important when the Alfvén radius R_A is of the order of the separation a (see Tout & Hall 1991). We adopt $R_A \simeq a$ and assume that the mass-loss rate from the binary star is proportional to

⁷ From the very rapid period decrease of $\dot{P}/P = 108.9 \pm 5.3 \times 10^{-7} \text{yr}^{-1}$, Kreiner et al. (2001) proposed that SV Cen is a semi-detached binary (Linnell & Scheick 1991) rather than a contact binary (Rucinski et al. 1992). Therefore, the most famous binary system SV Cen is still poorly understood (Sivak et al. 2010).

Table 7 Measured Fluxes for the Early-type Binary V2364 Cyg

λ (μm)	F_λ (Jy)	Error (Jy)	Bands	References
0.420	0.0963	± 0.0077	HIP: B_T	Høg et al. (2000)
0.532	0.134	± 0.012	HIP: V_T	Høg et al. (2000)
1.24	0.1120	± 0.0020	2MASS: J	Cutri et al. (2012)
1.65	0.0819	± 0.0021	2MASS: H	Cutri et al. (2012)
2.16	0.0534	± 0.0012	2MASS: K_s	Cutri et al. (2012)
0.505	0.106	± 0.004	Gaia: Gbp	Soubiran et al. (2018)
0.623	0.109	± 0.001	Gaia: G	Soubiran et al. (2018)
0.772	0.113	± 0.004	Gaia: Grp	Soubiran et al. (2018)
0.444	0.124	± 0.018	Johnson: B	Henden et al. (2016)
0.554	0.139	± 0.023	Johnson: V	Henden et al. (2016)
0.482	0.127	± 0.013	SDSS: g'	Henden et al. (2016)
0.625	0.142	± 0.019	SDSS: r'	Henden et al. (2016)
0.763	0.133	± 0.016	SDSS: i'	Henden et al. (2016)
0.477	0.120	± 0.060	PAN-STARRS $I: g$	Chambers et al. (2016)
0.748	0.136	± 0.068	PAN-STARRS $I: i$	Chambers et al. (2016)
0.613	0.132	± 0.066	PAN-STARRS $I: r$	Chambers et al. (2016)
0.865	0.1370	± 0.0685	PAN-STARRS $I: z$	Chambers et al. (2016)
0.960	0.1250	± 0.0625	PAN-STARRS $I: y$	Chambers et al. (2016)
0.444	0.107	± 0.006	Johnson: B	Lasker et al. (2008)
0.468	0.138	± 0.053	POSS-II: J	Lasker et al. (2008)
0.640	0.112	± 0.044	POSS-II: F	Lasker et al. (2008)
0.784	0.118	± 0.049	POSS-II: i	Lasker et al. (2008)
3.35	0.0221	± 0.0005	WISE: $W1$	Cutri et al. (2014)
4.6	0.0121	± 0.0002	WISE: $W2$	Cutri et al. (2014)
11.6	0.0021	± 0.0001	WISE: $W3$	Cutri et al. (2014)
22.1	0.00198		WISE: $W4$	Cutri et al. (2014)

Table 8 Early-type Contact Binaries with Period Variations

Star	Spectral	Period (d)	M_1 (M_\odot)	M_2 (M_\odot)	dP/dt ($\times 10^{-7}$ d yr $^{-1}$)	P_{mod} (yr)	References
LY Aur	O9+O9	4.0025	25.5	14.0	+7.2(± 0.7)	12.5	Mayer et al. (2013); Zhao et al. (2014)
BH Cen	B5	0.7916	9.4	8.3	+1.26(± 0.08)	50.3	Zhao et al. (2018); Leung et al. (1984)
SV Cen	B1	1.6597	9.6	7.7	-180.8(± 8.8)		Rucinski et al. (1992); Kreiner et al. (2001)
V593 Cen	B1	0.7553	6.2	5.9		50.9	Zhao et al. (2019); Lapasset et al. (1987)
V382 Cyg	O7.3V+O7.3V	1.8855	27.9	20.8	+4.4(± 0.2)	47.7	Qian et al. (2007); Yasarsoy & Yakut (2013)
V1073 Cyg	A9V	0.7859	1.73	0.52	-4.83(± 0.84)	82.7(± 3.6)	Pribulla et al. (2006); Tian et al. (2018)
V2364 Cyg	A7V	0.5921	1.80	0.55	-1.62(± 0.03)		This study
GU Mon	B1V	0.8966	8.79	8.58	-5.09(± 0.09)	34.2(± 0.6)	Yang et al. (2019); Lorenzo et al. (2016)
TU Mus	O7.5V+O9.5V	1.3873	23.5	15.3	+4.0(± 0.5)	47.73	Qian et al. (2007); Terrell et al. (2003)
IK Per	A2	0.6760	1.36	0.23	-2.50(± 0.09)	50.5	Zhu et al. (2005)
TY Pup	A9	0.8193	1.65	0.30	+0.58(± 0.01)	3.62	Sarotsakulchai et al. (2018); Gu et al. (1993)
V701 Sco	B5	0.7619	9.78	9.74	+4.31(± 0.86)	42.5(± 0.6)	Yang et al. (2019); Bell & Malcolm (1987)
CT Tau	B1V	0.6668	14.15	14.01		64.6(± 6.9)	Yang et al. (2019)

its mass, i.e., $\dot{M}_1 = M_1 \dot{M}/M$ and $\dot{M} = \dot{M}_1 + \dot{M}_2$. So, Equation (4) can be simplified as follows,

$$\frac{\dot{P}}{P} = \frac{2q^2 - q + 5}{q} \frac{\dot{M}}{M}. \quad (5)$$

Inserting \dot{P} , P , q , a and M into Equation (5), the mass-loss rate is estimated to be $\dot{M} = -8.62(\pm 0.02) \times 10^{-8}$ yr $^{-1}$ (i.e., $\dot{M}_1 = -6.53 \times 10^{-8}$ yr $^{-1}$ and $\dot{M}_2 = -2.08 \times 10^{-8}$ yr $^{-1}$). If we only consider conserved mass transfer from the more massive component to the less massive one, i.e., the second term in Equation (4), the mass loss rate for the primary should be $\dot{M}_1 = -7.32(\pm 0.02) \times 10^{-8}$ yr $^{-1}$. Whether or not conserved and non-conserved cases are implemented, most of the mass is lost from the more

massive component. This kind of mass loss via stellar wind may form a thin shell around the binary. Finally, this may cause infrared excess in the $W4$ band (Scaltriti et al. 1993; Busso et al. 1998). In the future, more infrared-excess EBs are very rewarding targets to investigate in terms of their mass loss from systems. High-precision spectroscopy and mid-eclipse times by photometry for V2364 Cyg are needed to identify our results.

Acknowledgements The authors would like to express many thanks for the anonymous referee's positive comments. This research is partially supported by the National Natural Science Foundation of China (Grant Nos. 11873003 & U1631108), Natural Science Research Key Program of Anhui Provincial Department of Education

(No. KJ2019A0954), the Outstanding Young Talents Program of Anhui Provincial Department of Education (Nos. gxyq2018161 & gxgnfx2019084), and Open Project Program of the Key Laboratory of Optical Astronomy, National Astronomical Observatories, Chinese Academy of Sciences. New photometry for V2364 Cyg was acquired by using the 80-cm and 85-cm telescopes at XLS of NAOC.

References

- Abbott, D. C. 1982, *ApJ*, 263, 723
- Akerlof, C., Amrose, S., Balsano, R., et al. 2000, *AJ*, 119, 1901
- Andersen, J. 1991, *A&ARv*, 3, 91
- Bell, S. A., & Malcolm, G. J. 1987, *MNRAS*, 226, 899
- Bonanos, A. Z. 2013, *IAUS*, 289, 173
- Boss, A. P. 2014, *ASS Meeting*, 223, id214.01
- Brickhouse, N. S., Dupree, A. K., & Hoogerwerf, R. 2005, *ESASP*, 560, 457
- Busso, M., Scaltriti, F., & Persi, P. 1998, *MNRAS*, 234, 445
- Csák, B., Kiss, L. L., Vinkó, J., & Alfaro, E. J. 2000, *A&A*, 356, 603
- Castor, J. I., Abbott, D. C., & Klein, R. I. 1975, *ApJ*, 195, 157
- Chambers, K. C., Magnier, E. A., Metcalfe, N., et al. 2016, *arXiv:1612.05560*
- Chen, W.-P., Sanchawala, K., & Chu, M. C. 2006, *AJ*, 131, 990
- Cutri, R. M., Skrutskie, M. F., van Dyk, S., et al. 2012, *VizieR Online Data Catalogue*, II/311
- Cutri, R. M., Skrutskie, M. F., van Dyk, S., et al. 2014, *VizieR Online Data Catalogue*, II/328
- Davidge, T. J. 1987, *AJ*, 94, 1169
- Davidge, T. J., & Milone, E. F. 1984, *ApJs*, 55, 571
- Denissenkov, P. A., & Vandenberg, D. A. 2003, *ApJ*, 598, 1246
- Djurasević, G., Baştürk, Ö., Latković, O., et al. 2013, *AJ*, 145, 80
- Djurasević, G., Ekmekçi, F., Albayrak, B. 2008, *RMxAA*, 44, 249
- Ekmekçi, F., Elmasli, A., Yilmaz, M., et al. 2012, *New Astron.*, 17, 603
- Erdem, A., & Öztürk, O. 2014, *MNRAS*, 441, 1166
- Gaia Collaboration, Brown, A. G. A., Vallenari, A., et al. 2018, *A&A*, 616, A1
- Gimenez, A., & Clausen, J. V. 1996, *ASPC*, 90, 44
- Gu, S., Yang, Yulan, Liu, Q., & Zhang, Z. 1993, *Ap&SS*, 203, 161
- He L., Wang S., Xu X.-J., et al. 2019, *RAA*, 19, 098
- Henden, A. A., Templeton, M., Terrell, D., et al. 2016, *VizieR Online Data Catalogue*, 2336, 0
- Hilditch, R. W. 2001, *An Introduction to Close Binary Stars* (London: Cambridge Univ. Press), p166
- Hoffmann, M., Stift, M. J., & Moffat, A. F. J. 1978, *PASP*, 90, 101
- Høg, E., Fabricius, C., Makarov, V. V., et al. 2000, *A&A*, 355, L27
- Hoňková, K., Juryšek, J., Lehký, M., et al. 2014, *Open Eur. J. of Var. Stars*, 165, 1
- Huang, F., Li, J.-Z., Wang, X.-F., et al. 2012, *Res. Astron. Astrophys.*, 12, 1585
- Hübsher, J. 2011, *Inf. Bull. Var. Stars*, 5984, 1
- Hübsher, J. 2013, *Inf. Bull. Var. Stars*, 6084, 1
- Hübsher, J. 2015, *Inf. Bull. Var. Stars*, 6152, 1
- Hübsher, J. 2016, *Inf. Bull. Var. Stars*, 6157, 1
- Hübsher, J., & Lehmann, P. 2012, *Inf. Bull. Var. Stars*, 6026, 1
- Hübsher, J., & Lehmann, P. 2013, *Inf. Bull. Var. Stars*, 6070, 1
- Hübsher, J., Lehmann, P., Monninger, G., et al. 2010, *Inf. Bull. Var. Stars*, 5941, 1
- Hübsher, J., Lehmann, P., & Walter, F. 2012, *Inf. Bull. Var. Stars*, 6010, 1
- Hurley, J. R., Tout, C. A., & Plos, O. R. 2002, *MNRAS*, 329, 897
- Jiang, D. 2020, *MNRAS*, 492, 2731
- Juryšek, J., Hoňková, K., Šmelcer, L., et al. 2017, *Open Eur. J. of Var. Stars*, 179, 1
- Kaluzny, J., & Krzeminski, W. 1993, *MNRAS*, 264, 785
- Kouzuma, S. 2019, *PASJ*, 71, 21
- Kopal, Z. 1959, *Close Binary Stars* (London: Chapman & Hall)
- Kreiner, J. M., Kim, C.-H., & Nha, I.-S. 2001, *An Atlas of O-C Diagrams of Eclipsing Binary Stars* (Cracow: Wydawnictwo Naukowe Akademii Pedagogicznej)
- Kurucz, R. L. 1993, *ApJS*, 40, 1
- Kwee, K. K., & van Woerden, H. 1956, *Bull. Astron. Inst. Netherlands, Bull. Astron. Ins. Nerth.*, 12, 327
- Lapasset, E., Gómez, M., & Clariá, J. J. 1987, *BAAA*, 33, 301
- Lasker, B. M., Lattanzi, M. G., McLean, B. J., et al. 2008, *AJ*, 136, 735
- Leung, K.-C., Sistero, R. F., & Zhai, D.-S. 1984, *AJ*, 89, 872
- Li, H.-L., Wei, J.-Y., Yang, Y.-G., & Dai, H.-F. 2016, *RAA (Research in Astronomy and Astrophysics)*, 16, 2
- Linnell, A., & Scheick, X. 1991, *ApJ*, 379, 721
- Liu, L., Qian, S.-B., & Xiong, X. 2018, *MNRAS*, 474, 5199
- Lorenzo, J., Negueruela, I., Vilardell, F., et al. 2016, *A&A*, 590, 45
- Lucy, L. B. 1967, *Z. Astrophys.*, 65, 89
- Luo, X., Wang, K., Zhang, X., et al. 2017, *AJ*, 154, 99
- Mayer, P., Drechsel, H., Stephenson, Y., & Šlechta, M. 2013, *A&A*, 559, A22
- Mestel, L., & Spruit, H. C. 1987, *MNRAS*, 226, 57
- Milone, E. F. 1968, *ApJ*, 73, 708
- Milone, E. F., Stagg, C. R., & Sugars, B. A. 1995, *AJ*, 109, 359
- Nagai, K. 2013, *Var. Star Bull. of Japan*, 55, 1
- Nanouris, N., Kalimeris, A., Antonopoulou, E., & Rovithis-Livaniou, H. 2011, *A&A*, 535, 126
- Nelson, R. H. 2008, *Inf. Bull. Var. Stars*, 5875, 1
- Nelson, R. H. 2017, *Inf. Bull. Var. Stars*, 6195, 1
- Nelson, R. H., Robb, R. M., Kaiser, D. H., & Billings, G. B. 2002, *Inf. Bull. Var. Stars*, 5285, 1
- Pietrzyński, G., Graczyk, D., Gieren, W., et al. 2013, *Nature*, 495, 76

- Pribulla, T., Rucinski, S. M., Lu, W., et al. 2006, *AJ*, 132, 769
- Qian, S.-B., Yuan, J.-Z., Liu, L., et al. 2007, *MNRAS*, 380, 1599
- Ruciński, S. M. 1969, *Acta Astronomica*, 19, 245
- Rucinski, S. M., Baade, D. Lu, W. X., & Udalski, A. 1992, *AJ*, 103, 573
- Sarotsakulchai, T., Qian, S.-B., Soonthornthum, B., et al. 2018, *AJ*, 156, 199
- Scaltriti, F., Busso, M., Ferrari-Toniolo, M., et al. 1993, *MNRAS*, 264, 5
- Siwak, M., Zoła, S., & Rucinski, S. 2010, *ASPC*, 435, 349
- Soubiran, C., Jasniewicz, G., Chemin, L., et al. 2018, *A&A*, 616, A7
- Stassun, K. G., & Torres, G. 2016, *AJ*, 152, 180
- Stępień 2006, *Acta Astron.*, 56, 199
- Terrell, D., Munari, U., Zwitter, T., et al. 2003, *AJ*, 126, 2988
- Tian, X.-M., Zhu, L.-Y., Qian, S.-B., et al. 2018, *RAA (Research in Astronomy and Astrophysics)*, 18, 20
- Tokovinin, A. 2008, *MNRAS*, 389, 925
- Torres, G., Andersen, J., & Gimenez, A. 2010, *A&ARv*, 18, 67
- Tout, C. T., & Hall, D. S. 1991, *MNRAS*, 253, 9
- Wang, J.-J., Qian, S.-B., Zhang, Y.-P., et al. 2015, *AJ*, 149, 164
- Wilson, R. E., & Devinney, E. J. 1971, *ApJ*, 166, 605
- Wilson, R. E., & van Hamme, W. 2014, *ApJ*, 780, 151
- Wilson, R. E., & van Hamme, W. 2015, *Computing Binary Star Observables*, <http://faculty.fiu.edu/~vanhamme/wdfiles/ebdoc2015-bf.pdf>
- Van Hamme, W. 1993, *AJ*, 106, 2096
- Von Zeipel, H. 1924, *MNRAS*, 84, 665
- Yakut, K., & Eggleton, P. P. 2005, *AJ*, 629, 1055
- Yasarsoy, B., & Yakut, K. 2013, *AJ*, 145, 9
- Yang, Y.-G., Qian, S.-B., Zhang, L.-Y., et al. 2013, *AJ*, 146, 35
- Yang, Y.-G., Yuan, H.-Y., & Dai, H.-F. 2019, *AJ*, 157, 111
- Yildiz, M., & Döğan, T. 2013, *MNRAS*, 430, 2029
- Zhang, X.-D., Qian, S.-B., & Liao, W.-P. 2020, *MNRAS*, 492, 4112
- Zhao, E.-G., Qian, S. B., Li, L., et al. 2014, *New Astron.*, 26, 112
- Zhao, E.-G., Qian, S.-B., Zejda, M., et al. 2018, *RAA (Research in Astronomy and Astrophysics)*, 18, 59
- Zhao, E.-G., Qian, S.-B., Soonthornthum, B., et al. 2019, *ApJL*, 871, L10
- Zhou, A.-Y., Jiang, X.-J., Zhang, Y.-P., et al. 2009, *RAA (Research in Astronomy and Astrophysics)*, 9, 349
- Zhu, L.-Y., Qian, S.-B., Soonthornthum, B., & Yang, Y.-G. 2005, *AJ*, 129, 2806
- Zinnecker, H. 2003, *Astrophysics and Space Science Library*, 299, 17